



## Studies on the performance of bentonite and its composite as phosphate adsorbent and phosphate supplementation for plant



Artik Elisa Angkawijaya<sup>a</sup>, Shella Permatasari Santoso<sup>b,c,\*</sup>, Vania Bundjaja<sup>c</sup>, Felycia Edi Soetaredjo<sup>b,c</sup>, Chintya Gunarto<sup>c</sup>, Aning Ayucitra<sup>b</sup>, Yi-Hsu Ju<sup>a,c,d</sup>, Alchris Woo Go<sup>a</sup>, Suryadi Ismadji<sup>b,c</sup>

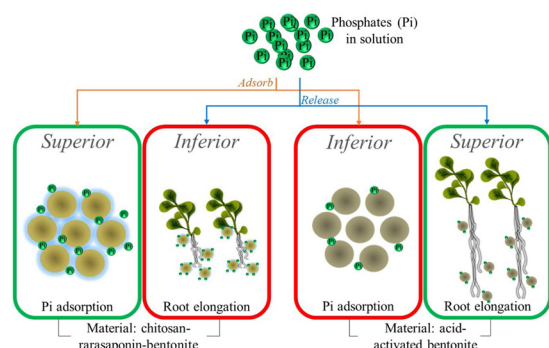
<sup>a</sup> Graduate Institute of Applied Science and Technology, National Taiwan University of Science and Technology, Taipei 10607, Taiwan

<sup>b</sup> Department of Chemical Engineering, Widya Mandala Catholic University Surabaya, Surabaya 60114, Indonesia

<sup>c</sup> Chemical Engineering Department, National Taiwan University of Science and Technology, Taipei 10607, Taiwan

<sup>d</sup> Chemical Engineering Department, National Taiwan University of Science and Technology, Taipei 10607, Taiwan

### GRAPHICAL ABSTRACT



### ARTICLE INFO

Editor: Daniel CW Tsang

Keywords:

Organo bentonite

Phosphate

Adsorption

Rarasaponin

Root elongation

### ABSTRACT

Organo-bentonite (OrB) was prepared by modifying bentonite with chitosan, and natural surfactant extracted from *Sapindus rarak* fruit. The physical alteration post-modification, performance of phosphates (Pi) adsorption, and possibility as a Pi-supplementation for plants of OrB were assessed and compared to acid-activated bentonite (AAB). The physical alteration due to modification of bentonite was characterized. SEM images were not indicating significant morphology differences between OrB and AAB. Existence of chitosan layers in OrB causes a decrease in basal spacing as characterized using XRD. The BET surface area of OrB was decreased compared to AAB due to pore coverage by chitosan. Adsorption studies reveal that OrB has a higher adsorption capacity towards Pi than AAB, which is 97.608 and 131.685 mg/g at 323 K for AAB and OrB, respectively. The H-shape isotherm curve indicates that chemisorption is dominantly controlling the adsorption. The isotherm and kinetics adsorption were well fitted to Langmuir and Pseudo-second order models, respectively. Performance of AAB and OrB as Pi-supplementation was assessed based on growth phenotypes of *Arabidopsis thaliana*; seedlings show that supplementation of Pi@AAB and Pi@OrB (at half doses) can promote primary root extension. These results also demonstrate the safety of direct disposal of the materials into the soil.

\* Corresponding author at: Department of Chemical Engineering, Widya Mandala Catholic University Surabaya, Surabaya 60114, Indonesia.

E-mail address: [shella\\_p5@yahoo.com](mailto:shella_p5@yahoo.com) (S.P. Santoso).

<https://doi.org/10.1016/j.jhazmat.2020.123130>

Received 6 April 2020; Received in revised form 4 June 2020; Accepted 4 June 2020

Available online 12 June 2020

0304-3894/ © 2020 Elsevier B.V. All rights reserved.

## 1. Introduction

The importance of phosphorus in biological functions and their essential role as a growth-limiting element for plants and animals is unquestionable (Angkawijaya et al., 2017; Gruber et al., 2013; F. Yang et al., 2019; Zhang et al., 2020). In nature, plants are the pivotal source of phosphorus for the animal. Inorganic phosphorus, such as phosphate (Pi), is the most readily available form for plant uptake (Młodzińska and Zboińska, 2016; Raghobhama, 1999; Yao et al., 2013). While at a certain level, the presence of Pi is crucial, contamination of extremely high levels in the aquatic environment can be very deteriorating. At a Pi level of 0.02 mg/L, it triggers a boom-growth of algae that leads to eutrophication and caused oxygen depletion (P. S. Kumar et al., 2019; R. Li et al., 2016). While under normal circumstances, Pi is very immobile in the soil, eutrophication is still considered as a persistent threat due to the disposal of Pi-containing wastewater. Reportedly, industrial wastewater from the H<sub>3</sub>PO<sub>4</sub> wet process, canned fish, dairy product, and anodized industry contain up to 5069 mg of Pi per liter of wastewater (Bacelo et al., 2019). Not limited to industrial waste, anthropogenic activities also contribute to increasing Pi levels in water bodies, i.e., domestic wastewater (5–20 mg/L), swine farm (100–987 mg/L), and urine (470–1070 mg/L) (Bacelo et al., 2019). Thus, a treatment process is needed to control the Pi level in the water body to avoid eutrophication.

Several methods have been developed to treat wastewater containing Pi, namely physical, chemical and biological treatment; but they might also be hybridized (G. Li et al., 2018; F. Xie et al., 2016; Q. Xie et al., 2017). In physical treatment (i.e., sorption), removal of Pi involves the use of adsorbent and adsorptive media with potential sorption capacity; adsorbent prepared from biochar, biomass, and clay minerals are widely used (Mdlalose et al., 2018; Peng et al., 2019; Robalds et al., 2016; F. Xie et al., 2016; Q. Xie et al., 2017; F. Yang et al., 2019; Q. Yang et al., 2018; Zhang et al., 2020). On the other hand, the Pi removal by chemical treatments usually involves precipitation and coagulation, which are carried out by the addition of chemicals such as aluminum sulfate, iron sulfate, and sodium aluminate (Mollah et al., 2004). Biological treatment involves the use of biofilm-forming organisms (i.e., algal-bacteria hybrid) to trap Pi and then precipitate it (Bunce et al., 2018). Various issues may arise from these treatments. Not only the added-chemical might be harmful to the environment, the efficiency of the treatment only served at high Pi concentration, and the recovery of Pi can be challenging. In biological treatment, time and the requirement for large processing area are the limiting factors. Meanwhile, the limitations of physical methods (particularly adsorption) revolve around the availability of suitable sorption matrix with high adsorption capacity. This limitation is relatively easier to address given the massive option of modifiable-material for adsorption matrix. Furthermore, the recoverability of Pi is one of the crucial points in its treatment method; this is since the natural production of Pi from phosphorous is a slow process. Therefore, exaggerate treatment (or removal) of Pi can lead to its scarcity. The advantage of adsorption is that the adsorbed substances can be easily recovered.

This study aims to develop an economical dual-purpose bentonite composite composed of natural materials that may act as a Pi-adsorbent and Pi-supplementation for plant nutrients. The natural materials such as bentonite, rarasaponin, and chitosan were used. The adsorptive ability of the synthesized composites against aqueous reactive Pi species was investigated. The novelty in this study derived from the utilization of environmentally friendly materials, thus facilitate direct disposal of post-adsorption bentonite to the soil without damaging effect on the environment. These findings will solve the drawback raised from the utilization of synthetic polymer-based adsorbents (e.g., PVC and resin) that are not readily degraded. Moreover, the potential of the Pi-loaded composites as a Pi-supplementation for plant growth was proven in this study.

## 2. Materials and methods

### 2.1. Materials

Bentonite used in this study was obtained from a mining site in Pacitan, East Java, Indonesia. Bentonite is chosen over other types of clay (such as struvite, ferrihydrite, and goethite) due to its abundance in many mining sites, especially in Indonesia. The bentonite was obtained in big chunks, which then crushed into a fine powder (+180/-200 mesh). The bentonite has cation exchange capacity of 45 meq/100 g; and dominantly composed of SiO<sub>2</sub> (62.0 %) followed by Al<sub>2</sub>O<sub>3</sub> (19.2 %), CaO (3.6 %), Fe<sub>2</sub>O<sub>3</sub> (3.0 %), Na<sub>2</sub>O (2.2 %), MgO (2.0 %), K<sub>2</sub>O (1.8 %), MnO (0.2 %), and TiO<sub>2</sub> (0.1 %). Rarasaponin was extracted from *Sapindus rarak* using methanol as a solvent (Putro et al., 2019).

Other chemicals used in this study are chitosan (85 % deacetylated) purchased from C.V. Nura Jaya, East Java, Indonesia; H<sub>2</sub>SO<sub>4</sub> (98 % purity), K<sub>2</sub>HPO<sub>4</sub> (99 % purity), and acetic acid glacial (CH<sub>3</sub>COOH, 99.85 % purity) purchased from Sigma Aldrich (St. Louis, USA) through a chemical distributor in East Java, Indonesia. Deionized water with 18.3 MΩ cm obtained from RDI Reverse Osmosis Deionizer System equipped with 50GPD UV ultrapure water maker and conductivity-meter (purity EC-410) were used throughout the experiment.

### 2.2. Preparation of adsorbents

Acid-activated bentonite (AAB) and organo-bentonite (OrB) were used as adsorbents. AAB was prepared by immersing bentonite into 1.5 M H<sub>2</sub>SO<sub>4</sub> solution for 2 h at 90 °C, as reported by Laysandra et al. (Laysandra et al., 2019). The AAB was pulverized to a fine powder (+80/-100 mesh) and kept in an airtight container. The OrB was prepared as follows: bentonite and rarasaponin (1:10 w/w) were mixed in 50 mL deionized water. The mixture was heated at 80 °C for 60 min under stirring 300 rpm, followed by irradiation using the microwave at a heating power of 700 W for 180 s (Santoso et al., 2017). Prior to the addition of chitosan solution to the rarasaponin-bentonite mixture, 1 wt % of chitosan powder was dissolved into 2.5 % (v/v) acetic acid solution and was stirred continuously at 80 °C for 60 min. The rarasaponin-chitosan-bentonite (OrB) mixture was then stirred for another 3 h, at 80 °C then dried in a 100 °C oven for 2 d. The obtained solid OrB was pulverized to a fine powder (+80/-100 mesh) and kept in an airtight container.

### 2.3. Adsorbent characterization

SEM analysis was conducted to collect the surface topography images. A JEOL JSM-6500 F (Japan) SEM at an accelerating voltage of 15.0 kV was used for the analysis. Prior to the analysis, the samples were coated with Pd/Pt coating using an auto fine coater JEOL JEC-3000FC (Japan). XRD analysis was performed to record the crystallinity pattern of the samples. The XRD measurements were conducted on a Bruker D2 Phaser diffractometer using Cu Kα radiation ( $\lambda = 1.5418 \text{ \AA}$ ). The surface functional group in adsorbent before and after adsorptions were investigated based on its Fourier Transform Infrared (FTIR) obtained from Shimadzu IRTracer-100, with KBr pellet was used as the background. Nitrogen (N<sub>2</sub>) adsorption and desorption analysis were carried out using Brunauer-Emmett-Teller (BET) BelsorpMax analyzer (Japan). The samples were degassed using Belprep-vacII at 150 °C for 4 h before the analysis to ensure total removal of all pre-occurring adsorbed species on the material surface.

### 2.4. Phosphate sorption

#### 2.4.1. Effect of pH

Pi solutions were prepared by dissolving K<sub>2</sub>HPO<sub>4</sub> in DI water at a concentration of 200 mg/L. The prepared Pi solution was distributed into a series of Erlenmeyer flask, each containing 50 mL solution. The

pH of each flask was adjusted to a certain pH using 0.1 M HCl or NaOH solution, between pH 3–12. 20 mg of adsorbent sample was introduced into a pH-adjusted solution. This test was done to assess the adsorption ability of the synthesized composite at different pH. The flasks were then put into a shaking water bath for 24 h. The data obtained from this analysis were used to determine the optimum pH for Pi adsorption using AAB and OrB.

#### 2.4.2. Adsorption isotherm

A series of capped Erlenmeyer flask containing 50 mL of Pi solution (200 mg  $K_2HPO_4$  in 1 L DI water) were prepared. The pH of the solution was adjusted to 6 and 8 before adsorption using AAB and OrB, respectively. A different mass of adsorbent samples (1, 5, 10, 20, 30, 40, 45, and 50 mg) was then introduced into each flask. The flasks were placed on a shaking water bath at a maintained temperature of 30, 40, or 50 °C. The adsorption was done for 24 h, then an aliquot of the solution was taken to determine the residual amount of Pi.

#### 2.4.3. Adsorption kinetics

20 mg of adsorbent sample was introduced into a series of capped Erlenmeyer flask containing Pi solution (200 mg  $K_2HPO_4$  in 1 L DI water). The pH of the solution was adjusted to 6 and 8 before adsorption using AAB and OrB, respectively. The adsorption kinetics of Pi onto the adsorbent sample was examined at three different temperatures of 30, 40, and 50 °C. An aliquot of the solution was taken from a flask at a different time interval (multiple of 15 min for the first 1 h, multiple of 30 min for the next 2 h, and 60 min) to determine the amount of Pi adsorbed.

#### 2.4.4. Residual Pi concentration measurement

The Pi-adsorbed composite was separated from the residual Pi solution by centrifugation at 3000 rpm for 3 min. Subsequently, the Pi solution was filtered using a 0.45  $\mu$ m pore size membrane syringe filter to remove the small adsorbent fragments or other small particles. The residual Pi concentration was then measured using the spectrophotometric method using ammonium molybdate-based reagent. The Pi containing solution will produce a colored solution with maximum absorbance at 880 nm. Details of the measurement procedure can be found elsewhere (Lowry and Lopez, 1946).

### 2.5. Adsorption data fitting

A graphing and fitting software, SigmaPlot version 12.5 build 12.5.0.38 (Systat Software, Inc.), was used to analyze the adsorption data. A data fitting based on adsorption mathematical models was performed using the dynamic curve fitting function; this is to examine the adsorption mechanism and behavior of Pi onto the adsorbent sample. The sum squared error ( $R^2$ ) calculated from the data fitting was evaluated to determine the best adsorption model that can well-correlate the data. Analysis of the statistical significance was determined using one-way ANOVA and Student's *t*-test by the GraphPad Prism program.

#### 2.5.1. Adsorption isotherm

The adsorption isotherm plots were constructed from the  $q_e$  versus  $C_e$  data points. The parameter  $q_e$  (mg/g) is the equilibrium amount of adsorbate adsorbed, and  $C_e$  (mg/L) is the residual amount of adsorbate at equilibrium. The value of  $q_e$  is calculated based on Eq. (1) as follow:

$$q_e = \frac{C_0 - C_e}{m} \times V \quad (1)$$

where  $C_0$  (mg/L) is the initial concentration of adsorbate,  $m$  (g) is the mass of adsorbent, and  $V$  (L) is the total volume of adsorption system.

The following multiple-parameters models (Table 1) were used to correlate the isotherm adsorption of Pi onto the adsorbents. As shown in many studies, Langmuir and Freundlich are the classic isotherm models

**Table 1**

The fitting models used for adsorption isotherm or kinetics, and the corresponding mathematical expression.

Fitting model	Equation	Fitting parameter (unit)	#Eq.
<i>Isotherm models</i>			
Langmuir <sup>a</sup>	$q_e = \frac{q_L K_L C_e}{1 + K_L C_e}$ $R_L = \frac{1}{1 + K_L C_0}$	$q_L$ (mg/g) $K_L$ (mg/L)	(2)
Freundlich <sup>b</sup>	$q_e = K_F C_e^{1/n_F}$	$K_F$ (mg/g)(L/mg) <sup>-n</sup> $n_F$	(3)
Redlich-Peterson <sup>c</sup>	$q_e = \frac{K_{RP} C_e}{1 + a_{RP} C_e^\beta}$	$K_{RP}$ (L/g) $a_{RP}$ (L/mg) $\beta$	(4)
Sips <sup>d</sup>	$q_e = \frac{q_S K_S C_e^{n_S}}{1 + K_S C_e^{n_S}}$	$q_S$ (mg/g) $K_S$ (L/g) $n_S$	(5)
<i>Kinetics models</i>			
Pseudo-first order <sup>e</sup>	$q_t = q_{e1}(1 - e^{-k_1 t})$	$q_{e1}$ (mg/g) $k_1$ (1/min)	(7)
Pseudo-second order <sup>f</sup>	$q_t = q_{e2} \left( \frac{q_{e2} k_2 t}{1 + q_{e2} k_2 t} \right)$	$q_{e2}$ (mg/g) $k_2$ (g/mg min)	(8)

<sup>a</sup> (Langmuir, 1916).

<sup>b</sup> (Freundlich, 1932).

<sup>c</sup> (Hamdaoui and Naffrechoux, 2007).

<sup>d</sup> (Belhachemi and Addoun, 2011; Hamdaoui and Naffrechoux, 2007).

<sup>e</sup> (Azizian, 2004; Lagergren, 1898).

<sup>f</sup> (Azizian, 2004; Ho and McKay, 1999).

which found to satisfy almost all adsorption systems (Belhachemi and Addoun, 2011; Hamdaoui and Naffrechoux, 2007). Langmuir model calculation assumes that the adsorbent surface is homogeneous. The constant  $q_L$  and  $K_L$  represent the maximum adsorption capacity and adsorption affinity constant, respectively. The dimensionless parameter  $R_L$  expresses the favorability of the adsorption. On the other hand, the Freundlich model is based on the assumption that the adsorbent surface is heterogeneous. The parameter  $K_F$  is a Freundlich parameter, which accounts for the adsorption capacity, while  $n_F$  is a dimensionless constant indicated the favorability of adsorption. Redlich-Peterson and Sips model is the hybrid of Langmuir and Freundlich model. The hybrid models are applicable for both homogeneous and heterogeneous systems; they also can be used to confirm the Langmuir and Freundlich model approaches. In the Redlich-Peterson model, the adsorption capacity is shown from the ratio of  $K_{RP}$  to  $a_{RP}$  ( $q_{RP} = K_{RP}/a_{RP}$ ). The value of parameter  $\beta$  can be used to determine the adsorption behavior. The adsorption obeys Langmuir as  $\beta = 1$ , and Freundlich as  $a_{RP} C_e^\beta > 1$ . In Sips model,  $q_S$  shows the adsorption capacity. The parameter  $K_S$  is a constant of equilibrium. Parameter  $n_S$  has a similar property with parameter  $\beta$  form Redlich-Peterson. The Sips model approaches Langmuir as  $n_S = 1$ , and Freundlich as  $C_e$  or  $K_S \rightarrow 0$ .

#### 2.5.2. Adsorption kinetics

The adsorption kinetics plots were constructed from the  $q_t$  versus  $t$  data points. The parameter  $q_t$  (mg/g) is the amount of adsorbate adsorbed at a certain time, and  $t$  (min) is the interval time of adsorption. The value of  $q_t$  is calculated based on Eq. (6) as follow:

$$q_t = \frac{C_0 - C_t}{m} \times V \quad (6)$$

where  $C_t$  (mg/L) is the residual concentration of adsorbate at time  $t$ .

In many kinetic adsorption studies, the Pseudo-first order and Pseudo-second order (Table 1) models are sufficiently satisfied with the adsorption data points. Both models can suggest solute adsorption rates in solutions (Ho and McKay, 1999; Lagergren, 1898). Both models provide an estimation of the equilibrium amount of adsorbate (solute) absorbed in the system under study, which is expressed in the parameters  $q_{e1}$  and  $q_{e2}$  for Pseudo-first order and Pseudo-second order, respectively. Furthermore, both models also provide the rate coefficient

values  $k_1$  (Pseudo-first order) and  $k_2$  (Pseudo-second order). The constant  $k_1$  is a combination of adsorption ( $k_{ads}$ ) and desorption ( $k_{des}$ ) rate constants, which linearly depend on the initial concentration of adsorbate. Differently, the constant  $k_2$  is a complex function of the initial concentration of adsorbate (Azizian, 2004).

The goodness of fit was analyzed using the adjusted determination coefficient ( $R_{adj}^2$ ) instead of the coefficient of determination ( $R^2$ ).  $R_{adj}^2$  can depict the goodness of fitting better than  $R^2$  since its calculation takes into account the degree of freedom from experimental data and also from the model.

## 2.6. Arabidopsis thaliana growth media supplementation

*A. thaliana* Columbia-0 ecotype was used as the model plant for the applicational study of Pi-adsorbed-OrB and AAB as a soil supplement. For this purpose, we prepare 4 different media: Pi containing media (P +), Pi starved media (P-), P- media supplemented by Pi-adsorbed-AAB (Pi@AAB), and P- media supplemented by Pi-adsorbed-OrB (Pi@OrB). The media were prepared according to previous publications (Angkawijaya et al., 2017; Estelle and Somerville, 1987; Nakamura et al., 2005) where its containing 0.8 % phosphate-free agar (Gelrite Pure, Kelco), 1% sucrose, and 20 mM MES buffer (pH 6.0), with 1 mM  $KH_2PO_4$  for P + or without  $KH_2PO_4$  for P- media. The *A. thaliana* seeds were germinated and grown on these 4 media under the continuous light condition at 22 °C. After 10 days, the seedlings grown on Pi@AAB and Pi@OrB were observed and compared to the one grown on P + or P- media. For this observation, 2 plates were prepared for each condition of the media, with 8 seeds were planted on each plate.

## 3. Results and discussion

### 3.1. Adsorbent characterizations

The obtained SEM images of AAB and OrB were depicted in Fig. 1. No significant surface morphology difference can be observed from

both images. Briefly, both AAB and OrB seem to have foliated structures in several areas and similarly rough-surface. However, in closer observation, the OrB (Fig. 1d) showed a slightly less-rough surface compared to AAB (Fig. 1b). This is caused by the presence of a thin layer of chitosan that envelops the clay particles.

The  $N_2$  adsorption-desorption curves of AAB and OrB are given in Fig. 2a, includes some features associated with mesoporous materials. It is observed that AAB has smaller pores than OrB; this is evident from continuous (and more extended) pore filling at lower relative pressures (at  $p/p^\circ \rightarrow 0$ ). The adsorption branch shows a low slope region, which suggests multilayer adsorption on the pores, this region is observed at  $p/p^\circ = 0.06 - 0.43$  for AAB and  $p/p^\circ = 0.03 - 0.44$  for OrB. The OrB appears to have a more extended low slope region, which implies that a more layered region formed by chitosan. The pore condensation region that forms a hysteresis is then observed. According to all observed features, the AAB and OrB have a Type IV isotherm with hysteresis loop type H4. The hysteresis loop type H4 indicates that the adsorbents contain complex pores, which causes the desorption process to be delayed (Sotomayor et al., 2018).

The calculated BET parameters, according to the  $N_2$  adsorption-desorption plot, are given in Table 2. The mean pore diameter of AAB is 6.392 nm, and OrB is 12.664 nm, which confirms the mesoporous pore size of the materials. AAB showed higher surface area ( $a_s = 162.350 \text{ m}^2/\text{g}$ ) than OrB ( $a_s = 32.029 \text{ m}^2/\text{g}$ ), indicates that the addition of chitosan might block the pores, thereby reducing the surface area. Despite the reduction of surface area, OrB provides additional functional group which promotes the adsorption capacity; this is shown in the functional groups characterization and adsorption experiments later.

The XRD crystallinity patterns of AAB and OrB are depicted in Fig. 2b. The XRD peaks of OrB emerge dominantly from the contribution of the bentonite. Peaks those correspond to montmorillonite, quartz, magnesite, and calcite were observed in both AAB and OrB sample. A single characteristic diffraction peak at  $2\theta = 2-10^\circ$  was observed for AAB and OrB, where this peak indicates the basal spacing

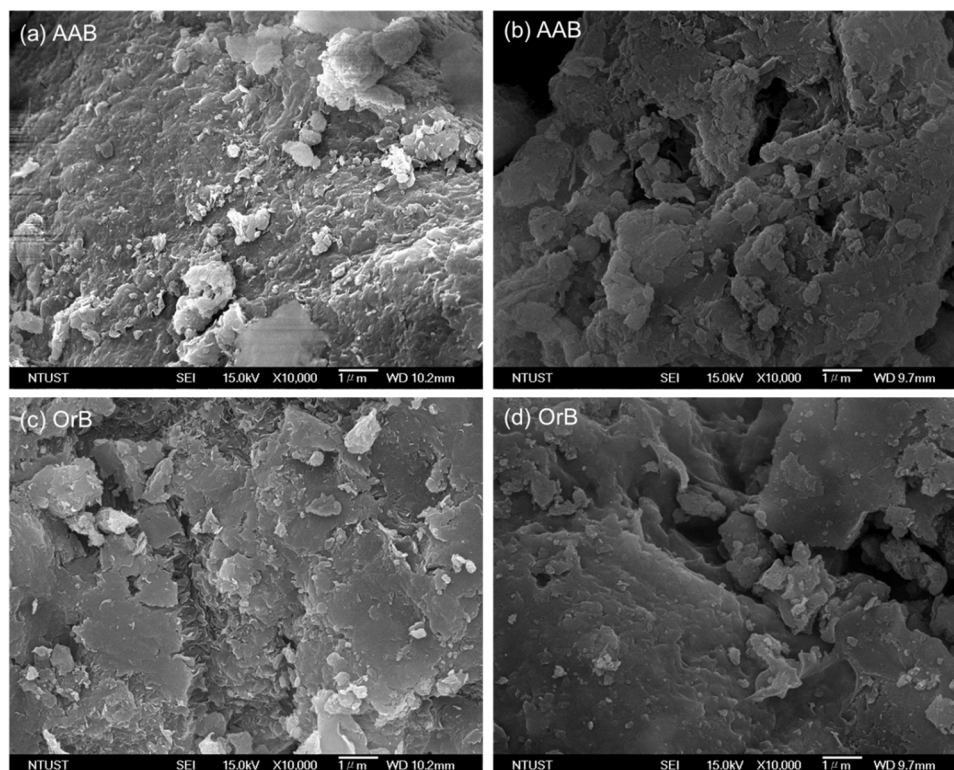


Fig. 1. SEM images of (a, b) acid-activated bentonite (AAB) and (c, d) chitosan-rarasaponin-bentonite (organo-bentonite, OrB) at different spots.

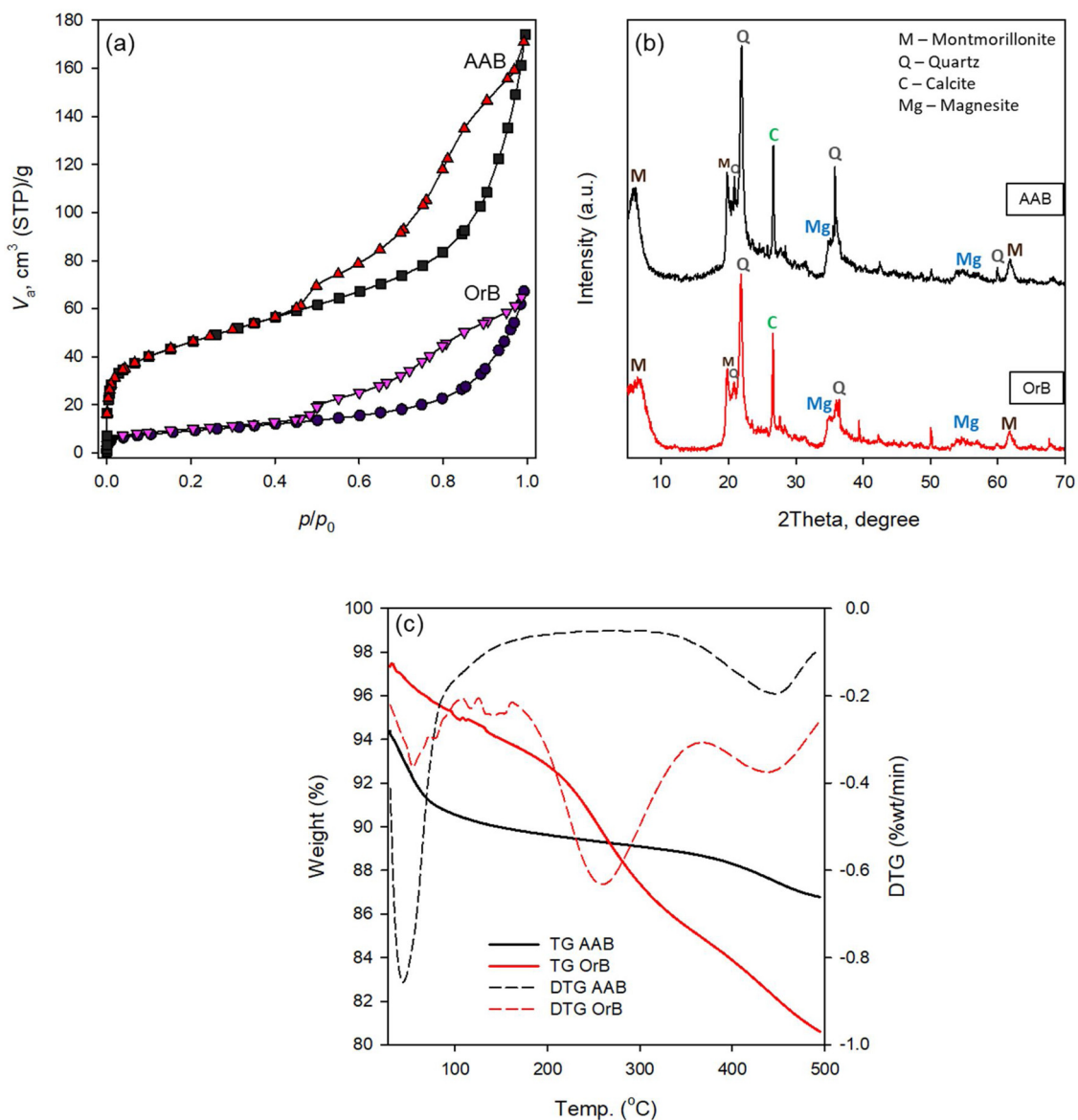


Fig. 2. (a) N<sub>2</sub> sorption plot, (b) XRD pattern, and (c) TG/DTG curve of acid-activated bentonite (AAB) and chitosan-rarasaponin-bentonite (organo-bentonite, OrB).

Table 2

BET parameters for acid-activated bentonite (AAB) and chitosan-rarasaponin-bentonite (organo-bentonite, OrB).

BET Parameter	Adsorbent	
	AAB	OrB
V <sub>m</sub> (cm <sup>3</sup> (STP)/g)	37.300	7.359
a <sub>s,BET</sub>	162.350	32.029
Mean pore diameter (nm)	6.392	12.664

(d-spacing) of the silicate layers. The d-spacing for AAB was measured at 2θ = 5.91°, with a value of 7.49 Å. The d-spacing for OrB was slightly shifted to the higher angle 2θ = 6.21° with the value of 7.12 Å. While the presence of surfactant postulated to provide an intercalation effect that may improve the d-spacing of bentonite (Kurniawan et al., 2011), rarasaponin-containing OrB has smaller d-spacing than AAB. This indicates that the incorporation of chitosan constricted the inter-layer galleries of AAB.

The thermal gravimetric analysis curves of AAB and OrB are illustrated in Fig. 2c, includes TG and DTG curves. The curves related to

AAB show mass losses of 4.23 % and 2.21 % in the temperature range of 30–140 °C and 320–500 °C, respectively. The endothermic peak in the range of 30–140 °C refers to the removal of water molecules that originated from surface humidity and water molecules coordinated to the interlayer of AAB. Meanwhile, the endothermic peak in the range of 320–500 °C occurs due to the de-hydroxylation of the silicate layer and removal of hydroxyl groups. Curves related to OrB show more stages of thermal degradation, specifically at the temperature of 30–100 °C (2.30 %), 110–160 °C (1.11 %), 170–360 °C (8.47 %), and 370–500 °C (4.23 %). The stages in the range of 30–100 °C and 110–160 °C correspond to the removal of humidity and coordinated water, respectively. The loss of water molecules occurs gradually due to the presence of chitosan, which forms more complex layers. The thermal degradation of chitosan signifies by the endothermic peak in the range of 170–360 °C (S. Kumar and Koh, 2012). The final stage of thermal degradation in the range of 370–500 °C occurs due to the same phenomenon in AAB, and also the degradation of the remaining chitosan residue (S. Kumar and Koh, 2012).

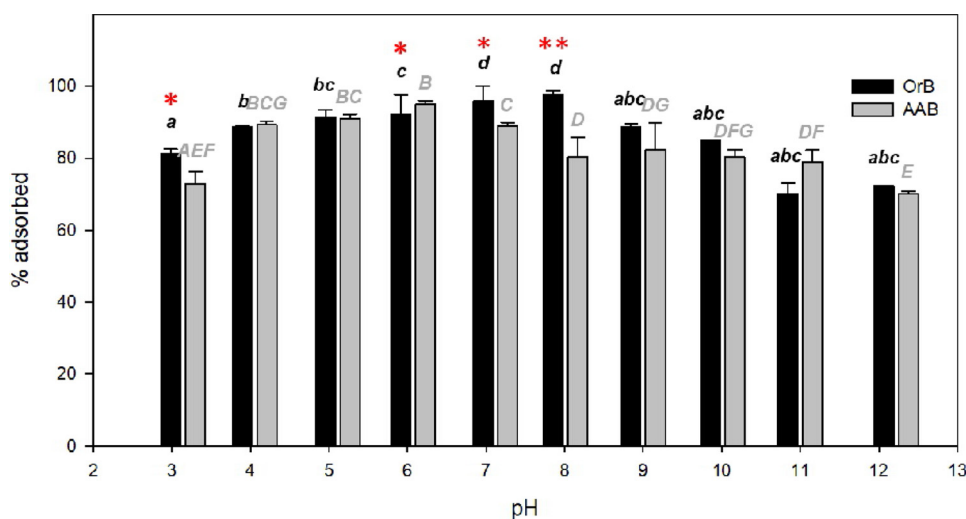


Fig. 3. Effect of pH on the adsorption (uptake) of phosphate using the investigated adsorbent, AAB, and OrB. Different letters indicate a significant difference with  $p < 0.05$ . The black letters indicate the significance of OrB uptake at various pH, while the gray capitalized letters represent the significance of pH in the adsorption capacity of AAB. The red asterisks indicate a significant comparison of OrB to AAB at the same pH by Student's  $t$ -test (\*\*  $p < 0.01$ ; \*  $p < 0.05$ ).

### 3.2. Effect of pH on the adsorption process

In this work, adsorption also refers to adsorbate uptake, since as the adsorbate molecules are being attached on adsorbent as they are adsorbed. pH value is an essential factor influencing many adsorption processes, adsorption, which takes place at an unsuitable pH will result in low adsorption efficiency. pH is closely related to the degree of ionization of the adsorbate and surface charge of adsorbent; the adsorption efficiency will be better if both have different charges. The surface charge of adsorbent can be determined from the pH-PZC value; where, positive surface charge occurs when pH solution  $<$  pH-PZC and vice versa (Milonjić et al., 1983). As determined using the pH-drift method, the pH-PZC of AAB is 5.16, and OrB is 7.23. Meanwhile, Pi is known as an anion, which has a negative charge at all pH range. The negative charge of Pi becomes higher as the pH solution increases.

Theoretically (judging from the pH-PZC adsorbent and anionic properties of the adsorbate), the optimal adsorption should fall within the acidic pH range (i.e., less than 5). However, the investigation result (Fig. 3) shows that the removal of Pi was optimized at pH of 5–6 for AAB and pH of 7–8 for OrB; that is close to the pH-PZC of each adsorbent. This is because, at pH  $>$  5, Pi as adsorbate is in the form of more negative species, that is,  $\text{HPO}_4^{2-}$ ; meanwhile at pH  $<$  5, the less negative  $\text{H}_2\text{PO}_4^-$  species were more dominant (Bacelo et al., 2019). The presence of more negative adsorbate species provides better electrostatic interaction with the adsorbent. Obviously, at more alkaline pH, both adsorbate and adsorbent possess negative charge; and thus, repulsive behavior is more dominant.

### 3.3. Adsorption mechanism of Pi onto adsorbents

FTIR analysis was carried out to get an idea of the mechanism of adsorption through the functional groups shifting before and after Pi adsorption, as shown in Fig. 4. For all samples, characteristic peaks of bentonite can be observed at 470, 524, 918, 1042, and 3618  $\text{cm}^{-1}$  which respectively refer to Si-O-Si bend, Al-O-Si bend, Al-Al-OH bend, Si-O-Si stretch, and Al(Mg)-O-H stretching. The incorporation of chitosan was displayed by the occurrence of C-N stretch and  $\text{NH}_2$  of amino group at 1096 and 1553  $\text{cm}^{-1}$  in OrB spectra. Additional peaks at 1382  $\text{cm}^{-1}$ , which refer to the P=O stretch of organic phosphates, can be observed in Pi@AAB and Pi@OrB; this confirmed the adsorption of Pi on AAB and OrB. Besides the peak of P=O stretch, Pi adsorption to OrB caused a shift of C-N stretch and  $\text{NH}_2$  of the amino group to 1088 and 1529  $\text{cm}^{-1}$ , respectively. After Pi adsorption, the peak of O-H stretch was intensified and shifted from 3432  $\text{cm}^{-1}$  for AAB and 3442 for OrB to 3409  $\text{cm}^{-1}$  (Pi@AAB) and 3417  $\text{cm}^{-1}$  (Pi@OrB). These peaks shift confirmed the involvement of the O-H group in the

adsorption of Pi onto AAB and OrB.

According to the analysis of pH-PZC and the shifting of functional groups (before and after Pi adsorption), the possible adsorption mechanism of Pi is illustrated in Fig. 5(a) for the AAB system and Fig. 5(b) for OrB system. In the AAB system, the excessive  $\text{H}^+$  ion due to acid activation of bentonite caused further protonation of the silanol groups of bentonites; thus, positive-charged groups occurred. The protonated groups then helped the adsorption of Pi through electrostatic interaction. Similar to AAB, the silanol group of bentonites in OrB also protonated in the solution. However, only minor protonation of the silanol group is occurring in OrB due to the absence of excessive  $\text{H}^+$  ions. While the addition of rarasaponin in OrB triggered intercalation of bentonite, their availability might not be the contributor to the enhanced Pi adsorption. Instead, the presence of chitosan molecules on OrB, which provides amine functional groups on the material surface. These amine groups can be protonated to  $-\text{NH}_3^+$  form, which later promotes the Pi binding through electrostatic interaction. The physical adsorption of Pi further supports this interaction onto the surface of OrB.

### 3.4. Adsorption isotherm

The effect of adsorption isotherm of Pi on AAB and OrB was investigated at three different temperatures, that is 303, 313, and 323 K. An endothermic adsorption behavior was observed from the adsorption using both tested adsorbents. Thus, the higher temperature was more favorable for the adsorption to proceed. Isotherm data fitting using several models was run prior to know the adsorption behavior and to quantify the isotherm parameters. A nonlinear fitting was conducted on the isotherm data; this is since a linear fitting may create data distortions during the transformation of data sets (Motulsky and Ransnas, 1987). The plots of isotherm data fitting into various models were presented in Fig. 6 for the AAB and OrB system.

The adsorption plots of Pi onto AAB and OrB show a one-step H-pattern curve, where high-affinity isotherm ( $q_e > > 0$ ) was observed at the beginning of the equilibrium curve. The H-pattern curve indicates that the adsorption system is dominated by chemisorption behavior and that electrostatic forces drive it. The occurrence of the (not strict) plateau at high adsorbate concentration indicates that the adsorbent saturation has occurred; and, it can be expected that the Langmuir and Langmuir-combination models (i.e., Redlich-Peterson and Sips) could satisfy the adsorption system. A good correlation of the isotherm data to the Langmuir and Langmuir-combination models also can be noted from the higher value of the adjusted determination coefficient ( $R_{adj}^2$ ) compared to Freundlich fitting (Table 3).

The highest adsorption capacity achieved from the batch adsorption

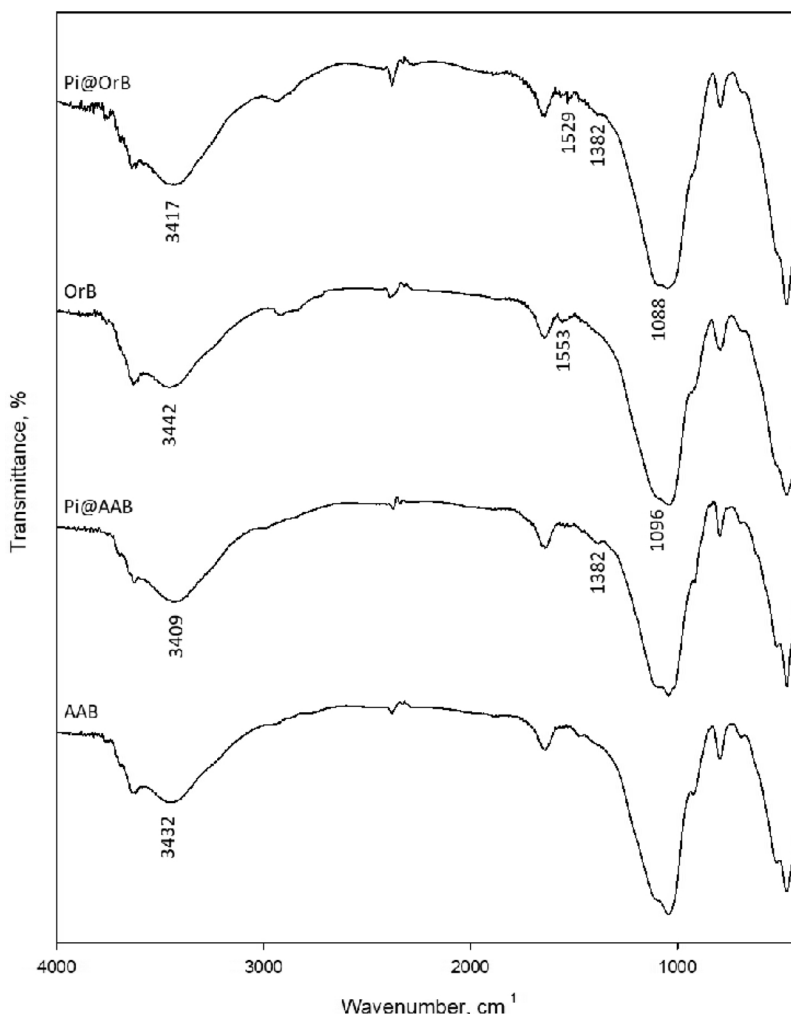


Fig. 4. FTIR spectra of acid-activated bentonite (AAB) and chitosan-rarasaponin-bentonite (organo-bentonite, OrB) before and after Pi adsorption (Pi@AAB and Pi@OrB).

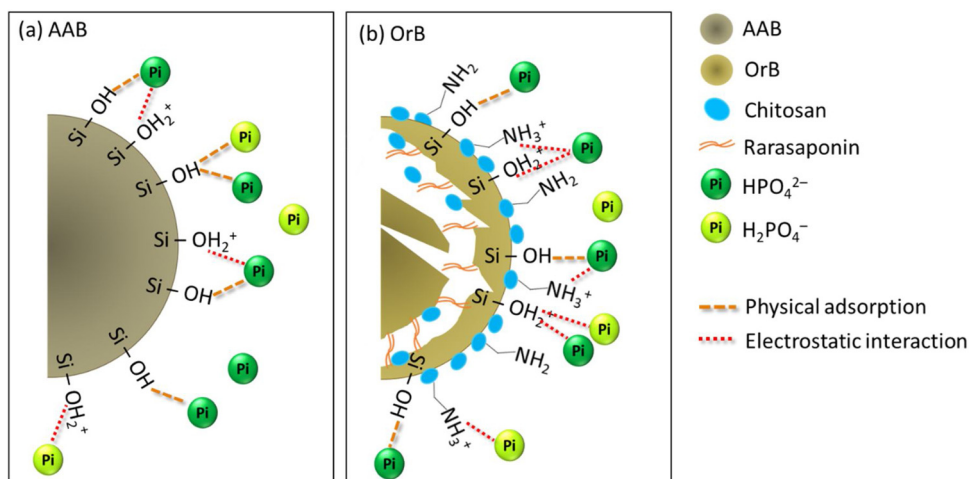


Fig. 5. Illustration of the possible mechanism of Pi adsorption onto (a) AAB and (b) OrB at pH close to pH-PZC (i.e., pH > 5).

experiment was recorded as  $q_{e(\text{exp})}$  value in Table 3. The  $q_{e(\text{exp})}$  showed that OrB could adsorb a higher amount of Pi compared to AAB at all investigated temperatures. The highest  $q_{e(\text{exp})}$  for AAB and OrB is achieved at the adsorption system at 323 K; that is 97.608 mg/g and 131.685 mg/g for AAB and OrB, respectively. Also, note that the value between  $q_{e(\text{exp})}$  and adsorption capacity calculated using the Langmuir

model ( $q_{\text{max}}$ ) and the Sips model ( $q_s$ ) has a difference of less than 10 %. This can be pointed out as a sign that the data points in the batch adsorption experiment have almost reached the plateau condition. Meanwhile, the Redlich-Peterson model is failed to describe the maximum adsorption capacity of the system under investigation. This can be seen from the difference in the value of  $q_{\text{RP}}$  which is very far

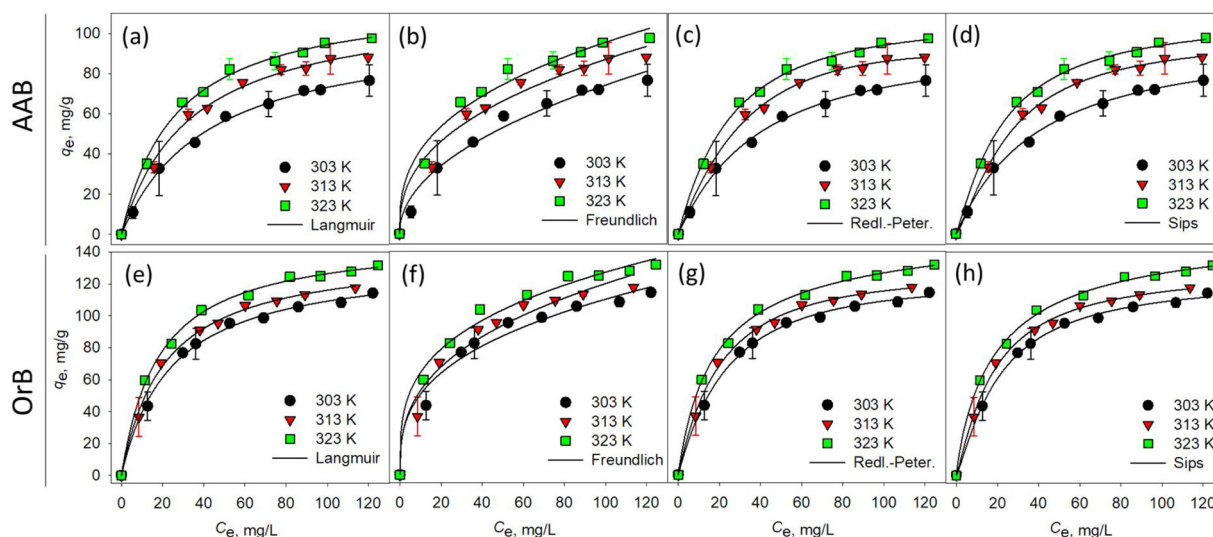


Fig. 6. Phosphate (Pi) adsorption isotherm data ( $C_0 = 200 \text{ mg/L}$ ,  $T = 303, 313, 323 \text{ K}$ ) and fitting of: (a-d) acid-activated bentonite (AAB) at pH of 6, and (e-f) organo-bentonite (OrB) at pH of 8.

different from  $q_E(\text{exp})$ .

It has been evaluated that Pi adsorption onto AAB and OrB obeys Langmuir and Sips model. The Sips model is a three-parameters model that does not provide a direct insight to justify the experimental data. The models can be used to confirm the satisfactory of the Langmuir or Freundlich fitting. Based on the fitting results, the  $n_S$  value (Sips model) of all the adsorption systems is close to 1, indicates their better approach to the Langmuir model. Furthermore, the  $K_S$  of the Sips model does not show zero value, which confirms the Langmuir approach (Belhachemi and Addoun, 2011; Hamdaoui and Naffrechoux, 2007).

Although it has been evaluated that Pi adsorption on AAB and OrB obeys the Langmuir model, it is still interesting to evaluate each parameter of the other models to reveal the suitability of the adsorption system with Langmuir. The  $n_F$  parameter of the Freundlich model shows a value in the range of 2–10, which indicates favorable adsorption. The adsorption system is not favorable when the  $n_F$  value is less than 2 (Hamdaoui and Naffrechoux, 2007). The favorability of the adsorption also can be assessed from the  $R_L$  value of the Langmuir model. The  $R_L$  values of all systems lie between  $0 < R_L < 1$ , indicating that the adsorption is favorable (Hamdaoui and Naffrechoux, 2007). Redlich-

Peterson is a three-parameter model; similar to the Sips model, and it does not provide a direct insight to justify the experimental data. The exponent  $\beta$  values of the Redlich-Peterson model are close to 1, indicates a better approach to the Langmuir model (Belhachemi and Addoun, 2011; Hamdaoui and Naffrechoux, 2007).

The utilization of bentonite-based materials to adsorb Pi has been reported in several studies (Table 4). The most recent studies proposed modification of bentonite using metal ions to increase the adsorption capacity of Pi. For instance, some transition metal ions were used to modify bentonite, including Co, Ni, and Fe. The Co-, Ni-, and Fe-modified bentonite can adsorb Pi up to 46.95, 29.07, and 20.88 mg/g, while unmodified bentonite is only able to adsorb 6.57 mg/g (Mdalose et al., 2018). Modification of bentonite using Zr metal ion was reported to have an adsorption capacity of 13.40 mg Pi/g (Lin et al., 2018). Further modification of Zr- bentonite using Mg metal ion succeeded in increasing the adsorption capacity of Pi to 16.00 mg/g (Lin et al., 2020). Modification of bentonite using metal ions is proven to be able to increase the adsorption capacity of Pi. Still, the buildup (and disposal) of materials containing metal ions may have the potential to damage the environment and can cause metal poisoning. The use of natural

Table 3  
The calculated parameter values of the isotherm fitting models.

Model	Parameter	AAB			OrB		
		303 K	313 K	323 K	303 K	313 K	323 K
–	$q_E(\text{exp})$	76.502	88.121	97.608	114.212	117.633	131.685
Langmuir	$q_{\text{max}}$	83.816	115.387	119.255	135.425	140.238	149.399
	$K_L$	0.024	0.030	0.038	0.042	0.048	0.055
	$R_L$	0.172	0.143	0.116	0.106	0.094	0.083
	$R_{\text{adj}}^2$	0.998	0.994	0.996	0.997	0.997	0.998
	SSE	12.978	34.654	28.203	30.469	34.714	31.583
Freundlich	$K_F$	7.851	14.041	18.006	23.156	23.357	32.363
	$n_F$	2.049	2.525	2.762	2.958	2.817	3.367
	$R_{\text{adj}}^2$	0.979	0.975	0.976	0.975	0.969	0.987
	SSE	112.869	153.682	179.247	240.573	347.317	166.119
	$q_{\text{RP}}$	136.588	188.667	377.714	139.389	199.600	219.455
Redlich-Peterson	$\beta$	1.059	1.087	1.244	0.956	1.071	1.093
	$R_{\text{adj}}^2$	0.997	0.996	0.996	0.997	0.997	0.997
	SSE	12.299	23.671	18.694	28.176	27.652	22.455
	$q_S$	99.221	99.562	110.262	124.726	130.496	156.920
	$K_S$	0.021	0.012	0.025	0.025	0.034	0.069
Sips	$n_S$	1.060	1.355	1.182	1.219	1.171	0.892
	$R_{\text{adj}}^2$	0.997	0.997	0.997	0.998	0.998	0.998
	SSE	12.082	16.320	20.595	16.907	22.188	21.111

**Table 4**  
Pi adsorption performance on modified bentonite (Bent) adsorbents.

Adsorbent	Adsorption experiment			Ref
	Condition	$Q_{max}$ (mg/g)	Best fitted model	
Fe-Bent	pH = 3 $C_0 = 1000$ mg/L $KH_2PO_4$	20.88 (at 298 K)	Langmuir	(Mdlalose et al., 2018)
Ni-Bent		29.07 (at 298 K)		
Co-Bent		46.95 (at 298 K)		
Zr-Bent	pH = 7	13.40 (at 298 K)	Langmuir	(Lin et al., 2020)
ZrMg-Bent		16.00 (at 298 K)		
Fe-Al-Bent	pH = 6.5 $C_0 = 250$ mg/L $KH_2PO_4$	8.33 (at 298 K)	Langmuir-Freundlich	(Yaghoobi-Rahni et al., 2017)
Acid and heat-treated Bent	pH = 3 $C_0 = 150$ mg/L $KH_2PO_4$	20.37 (at 318 K)	Langmuir	(Tanyol et al., 2015)
AAB	pH = 6 $C_0 = 200$ mg/L $KH_2PO_4$	76.502 (at 303 K)	Langmuir	This study
		88.121 (at 313 K)		
		97.608 (at 323 K)		
OrB	pH = 8 $C_0 = 200$ mg/L $KH_2PO_4$	114.212 (at 303 K)	Langmuir	This study
		117.633 (at 313 K)		
		131.685 (at 323 K)		

components as adsorbents for Pi (i.e., OrB) is still rare or has not been reported, which is highlighted in this study. OrB can be more environmentally friendly than metal-modified bentonite adsorbents, the natural component used to prepare OrB allows direct disposal to the ground without damage potential. In addition, the adsorption capacity of Pi provided by OrB (i.e., 131.685 mg/g) is much higher than that of metal-modified and unmodified bentonite; this shows the superiority of OrB in Pi adsorption from aqueous solution.

### 3.5. Adsorption kinetics

Pseudo-first order and Pseudo-second order fitting were used to quantify the rate of adsorption (Ikhtiyarova et al., 2012). The adsorption kinetics plot (Fig. 7) indicates rapid adsorption in the first 30 min. This phenomenon is very common for adsorption systems that begin with high adsorbate concentrations. Rapid adsorption at the beginning of adsorption also shows that the electrostatic force drives the interaction between the adsorbent and adsorbate. Adsorption occurs instantly because the active sites of the ligand are still empty and have a high affinity for the opposite-charged adsorbate molecule (Q. Yang et al., 2018). Then, the adsorption rate starts to slow down, and a plateau is reached along with the reduction of the active sites of the adsorbent.

Based on the kinetics models fitting results (Table 5), it is indicated that the adsorption system of Pi onto AAB and OrB obey the Pseudo-second order instead of the Pseudo-first order. This is shown from the

**Table 5**

The calculated parameter values of the isotherm fitting models.

Model	Parameter	AAB			OrB		
		303 K	313 K	323 K	303 K	313 K	323 K
–	$q_e$ (exp)	45.123	59.622	71.648	82.165	91.253	104.201
Pseudo-first order	$q_{e1}$	44.192	58.320	69.575	81.541	90.117	102.148
	$k_1$	0.117	0.140	0.148	0.170	0.193	0.174
	$R_{adj}^2$	0.994	0.998	0.996	0.999	0.998	0.996
Pseudo-second order	$q_{e2}$	45.927	59.920	71.437	82.879	91.523	104.321
	$k_2$	0.006	0.007	0.008	0.009	0.010	0.010
	$R_{adj}^2$	1.000	0.998	0.999	0.999	0.996	1.000

$R_{adj}^2$  value, which is close to 1 for the Pseudo-second order. Moreover, the predicted adsorption capacity based on the Pseudo second-order model ( $q_{e2}$ ) shows a value close to the adsorption capacity of the experimental results ( $q_e$  (exp)). Temperature variations also appear to affect the adsorption, where an increase in temperature allows adsorption to occur faster and more favorable.

### 3.6. Root growth in Pi media

*A. thaliana* was used as the model plant to assess the applicability of Pi-loaded composites as Pi-supplementation for plant growth. One of the most apparent phenotypical adaptive response in Pi-starved plant is displayed by the suppression of the primary root growth along with the

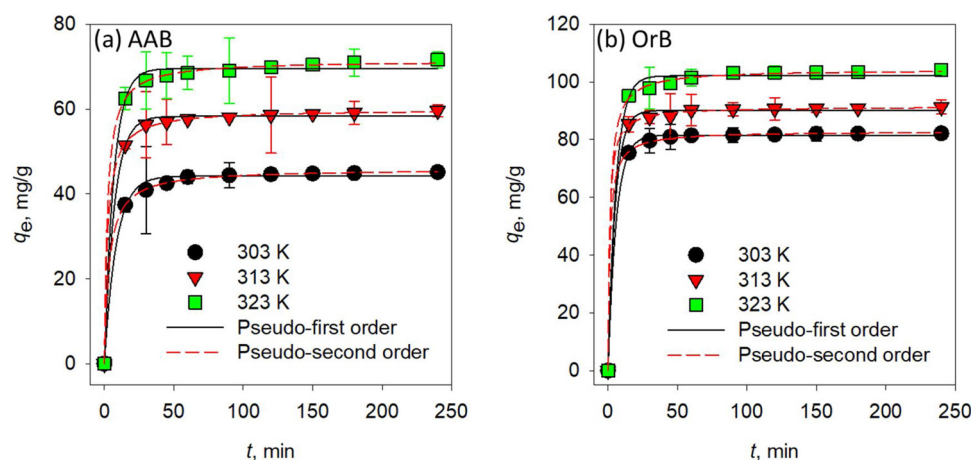


**Fig. 7.** Phosphate (Pi) adsorption kinetics data ( $C_0 = 200$  mg/L,  $T = 303, 313, 323$  K) and fitting of: (a) acid-activated bentonite (AAB) at pH of 6, and (b) organo-bentonite (OrB) at pH of 8.

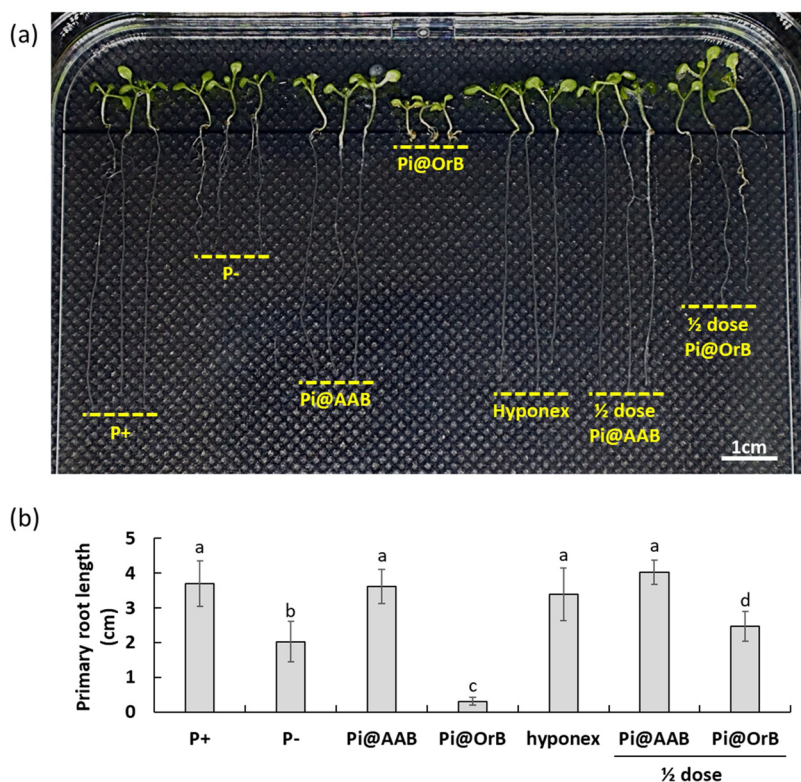


**Fig. 8.** Growth observation of *Arabidopsis thaliana* 10 days old seedlings grown on various media. (a) Images of 10 days old seedlings. (b) Primary root length of the seedlings. From left to right: normal media (P+), phosphate-starved media (P-), Pi@AAB-supplemented phosphate-starved media (Pi@AAB), Pi@OrB-supplemented phosphate-starved media (Pi@OrB), commercial fertilizer (Hyponex), and half dose of Pi@AAB and Pi@OrB. Different letters indicate a significant difference with  $p < 0.05$ .

promotion of lateral root and root hair growth (Angkawijaya et al., 2017; Bernardo et al., 2018; Péret et al., 2011). To observe the root growth, *A. thaliana* seeds were grown on control media (P+ and P-), bentonite-supplemented media for 10 days.

To even up the amount of Pi source in bentonite-supplemented media, 84 mg Pi@AAB and 66 mg Pi@OrB were added to 50 mL phosphate-free media. As presented in Fig. 8, the seedlings grown on Pi@AAB had longer roots than P- seedling and were very slightly shorter than the one grown on P+. In contrast, the supplementation of full dose Pi@OrB (66 mg) caused severe growth retardation in root as well as aerial tissue, which shows pale green leaves. These impaired growths might be due to the presence of surfactant (i.e., rarasaponin) in excess, thus adversely affect seed germination, root growth, and overall plant biomass (Gálvez et al., 2019; Parr and Norman, 1964). The occurrence of  $1.32 \text{ g L}^{-1}$  rarasaponin in Pi@OrB media is more than 2-fold higher than the recommended surfactant usage for the plant ( $< 0.65 \text{ g L}^{-1}$ ) (Gálvez et al., 2019). To comply with the recommended surfactant concentration, media with half dosage of Pi@OrB were prepared. Interestingly, at a half dosage of Pi@OrB supplementation, the primary root length of the seedlings was significantly longer than the one grown on P- media and showed partial complementation of primary root growth. Thus confirm the toxic effect of excessive surfactant (here rarasaponin) to the *A.thaliana* growth. In this work, commercial fertilizer (Hyponex N:P:K 10:30:20) was used to evaluate the applicability of Pi@AAB and Pi@OrB as plant fertilizer. As displayed in Fig. 8, full- and half-dose Pi@AAB showed a comparable growth as the one grown on Hyponex-containing media. Pi@OrB supplementation showed more defect root growth compared to Pi@AAB; however, root lengthening in Pi@OrB-supplemented media (especially at 1/2 dose) was better than the one grown on P- media.

#### 4. Conclusion

Organo-bentonite (OrB) was prepared by modifying bentonite with rarasaponin-surfactant and chitosan. The current study demonstrates that OrB is a potential adsorbent for the removal of phosphate

compounds (Pi) from aqueous solutions. OrB has higher adsorption capacity towards Pi compared to acid-activated bentonite (AAB). pH slightly affected the adsorption of Pi onto AAB and OrB. Adsorption isotherms of Pi on AAB and OrB were investigated and modeled using several isotherm models. The investigated adsorption systems show a good fitting with the Langmuir model. Analysis of the parameters of the other isotherm models shows conformity with the Langmuir model. Adsorption kinetics study reveals a rapid Pi removal at the beginning implies that the adsorption is driven by electrostatic force and supported by the physical adsorption. A good fitting of kinetics data to Pseudo-second order models shows that the adsorption rate is a complex function of initial adsorbate concentration. Pi@AAB, at full- and half- dose, can be used as Pi source to promote the primary root elongation of *Arabidopsis thaliana*. A full-dose Pi@OrB was shown to suppress the primary root elongation, but, a half-dose Pi@OrB can promote root elongation better than the Pi-starvation media. These findings confirm the applicability of Pi@AAB and Pi@OrB as Pi supplements; however, the effect of supplementation on the actual soil can be different. There are many factors in the actual soil (i.e., pH, humidity, organic matters, micro- and macronutrient content) that affect plant growth. Thus, more comprehensive studies are needed to examine the effects of the materials supplementation on the soil.

#### CRediT authorship contribution statement

**Artik Elisa Angkawijaya:** Investigation, Funding acquisition, Writing - original draft. **Sheila Permatasari Santoso:** Investigation, Conceptualization, Data curation, Writing - review & editing. **Vania Bundjaja:** Formal analysis, Data curation. **Felycia Edi Soetaredjo:** Resources, Writing - review & editing. **Chintya Gunarto:** Formal analysis. **Aning Ayucitra:** Formal analysis. **Yi-Hsu Ju:** Supervision. **Alchris Woo Go:** Conceptualization. **Suryadi Ismadji:** Supervision, Project administration, Funding acquisition.

## Acknowledgments

The authors thank Ms. Cam Van Nguyen and Dr. Anh Hai Ngo (Institute of Plant and Microbial Biology, Academia Sinica) for their support with plant growth media. The authors gratefully acknowledge financial support from the Widya Mandala Surabaya Catholic University through Internal Research Grant, National Science Council of Taiwan (MOST 108-2218-E-011-033), and National Taiwan University of Science and Technology (101H451403).

## References

- Angkawijaya, A.E., Nguyen, V.C., Nakamura, Y., 2017. Enhanced root growth in phosphate-starved *Arabidopsis* by stimulating *de novo* phospholipid biosynthesis through the overexpression of *LYSOPHOSPHATIDIC ACID ACYLTRANSFERASE 2 (LPAT2)*. *Plant Cell Environ.* 40 (9), 1807–1818. <https://doi.org/10.1111/pce.12988>.
- Azizian, S., 2004. Kinetic models of sorption: a theoretical analysis. *J. Colloid Interf. Sci.* 276, 47–52. <https://doi.org/10.1016/j.jcis.2004.03.048>.
- Bacelo, H., Pintor, A.M.A., Santos, S.C.R., Boaventura, R.A.R., Botelho, C.M.S., 2019. Performance and prospects of different adsorbents for phosphorus uptake and recovery from water. *Chem. Eng. J.* 381, 122566. <https://doi.org/10.1016/j.cej.2019.122566>.
- Belhachemi, M., Addoun, F., 2011. Comparative adsorption isotherms and modeling of methylene blue onto activated carbons. *Appl. Water Sci.* 1, 111–117. <https://doi.org/10.1007/s13201-011-0014-1>.
- Bernardo, M.P., Guimarães, G.G.F., Majaron, V.F., Ribero, C., 2018. Controlled release of phosphate from layered double hydroxide structures: dynamics in soil and application as smart fertilizer. *ACS Sustain. Chem. Eng.* 6 (4), 5152–5161. <https://doi.org/10.1021/acssuschemeng.7b04806>.
- Bunce, J.T., Ndam, E., Ofiteru, I.D., Moore, A., Graham, D.W., 2018. A review of phosphorus removal technologies and their applicability to small-scale domestic wastewater treatment systems. *Front. Environ. Sci.* 6, 8. <https://doi.org/10.3389/fenvs.2018.00008>.
- Estelle, M.A., Somerville, C., 1987. Auxin-resistant mutants of *Arabidopsis thaliana* with an altered morphology. *Mol. Gen. Genet.* 206, 200–206. <https://doi.org/10.1007/BF00333575>.
- Freundlich, H., 1932. Of the adsorption of gases. Section II. Kinetics and energetics of gas adsorption. Introductory paper to section II. *Trans. Faraday Soc.* 28, 195–201. <https://doi.org/10.1039/TF9322800195>.
- Gálvez, A., López-Galindo, A., Peña, A., 2019. Effect of different surfactants on germination and root elongation of two horticultural crops: implications for seed coating. *N. Z. J. Crop Hortic. Sci.* 47 (2), 83–98. <https://doi.org/10.1080/01140671.2018.1538051>.
- Gruber, B.D., Giehl, R.F.H., Friedel, S., Wirén, N., 2013. Plasticity of the *Arabidopsis* root system under nutrient deficiencies. *Plant Physiol.* 163, 161–179. <https://doi.org/10.1104/pp.113.218453>.
- Hamdaoui, O., Naffrechoux, E., 2007. Modeling of adsorption isotherms of phenol and chlorophenols onto granular activated carbon Part I. Two-parameter models and equations allowing determination of thermodynamic parameters. *J. Hazard. Mater.* 147, 381–394. <https://doi.org/10.1016/j.jhazmat.2007.01.021>.
- Ho, Y.S., McKay, G., 1999. Pseudo-second order model for sorption processes. *Process Biochem.* 34 (5), 451–465. [https://doi.org/10.1016/S0032-9592\(98\)00112-5](https://doi.org/10.1016/S0032-9592(98)00112-5).
- Ikhtiyarova, G.A., Ozcan, A.S., Gok, O., Ozcan, A., 2012. Characterization of natural- and organobentonite by XRD, SEM, FT-IR and thermal analysis techniques and its adsorption behaviour in aqueous solutions. *Clay Miner.* 47, 31–44. <https://doi.org/10.1180/claymin.2012.047.1.31>.
- Kumar, S., Koh, J., 2012. Physicochemical, optical and biological activity of chitosan-chromone derivative for biomedical applications. *Int. J. Mol. Sci.* 13 (5), 6102–6116. <https://doi.org/10.3390/ijms13056102>.
- Kumar, P.S., Korving, L., Loosdrecht, M.C.M.v., Witkamp, G.-J., 2019. Adsorption as a technology to achieve ultra-low concentrations of phosphate: research gaps and economic analysis. *Water Res.* 4 (1), 100029. <https://doi.org/10.1016/j.wroa.2019.100029>.
- Kurniawan, A., Sutiono, H., Ju, Y.-H., Soetaredjo, F.E., Ayucitra, A., Yudha, A., Ismadji, S., 2011. Utilization of rarasaponin natural surfactant for organo-bentonite preparation: application for methylene blue removal from aqueous effluent. *Microporous Mesoporous Mater.* 142 (1), 184–193. <https://doi.org/10.1016/j.micromeso.2010.11.032>.
- Lagergren, S., 1898. About the theory of so-called adsorption of soluble substances. *Kungl. Svenska Vetenskapskad. Handl.* 24, 1–39.
- Langmuir, I., 1916. The constitution and fundamental properties of solids and liquids. Part I. Solids. *J. Am. Chem. Soc.* 38 (11), 2221–2295. <https://doi.org/10.1021/ja02268a002>.
- Laysandra, L., Ondang, I.J., Ju, Y.-H., Ariandini, B.H., Mariska, A., Soetaredjo, F.E., et al., 2019. Highly adsorptive chitosan/saponin-bentonite composite film for removal of methyl orange and Cr(VI). *Environ. Sci. Pollut. Res.* 26, 5020–5037. <https://doi.org/10.1007/s11356-018-4035-2>.
- Li, R., Wang, J.J., Zhou, B., Awasthi, M.K., Ali, A., Lahori, Z.Z.A.H., Mahar, A., 2016. Recovery of phosphate from aqueous solution by magnesium oxide decorated magnetic biochar and its potential as phosphate-based fertilizer substitute. *Bioresour. Technol.* 215, 209–214. <https://doi.org/10.1016/j.biortech.2016.02.125>.
- Li, G., Hao, Y., Qi, L., Li, Y., 2018. Study on recovery source of phosphorus from toilet Water by electrochemistry. In: Paper Presented at the 2nd International Symposium on Resource Exploration and Environmental Science. Ordos, China.
- Lin, J., Jiang, B., Zhan, Y., 2018. Effect of pre-treatment of bentonite with sodium and calcium ions on phosphate adsorption onto zirconium-modified bentonite. *J. Environ. Manage.* 217, 183–195. <https://doi.org/10.1016/j.jenvman.2018.03.079>.
- Lin, J., He, S., Zhan, Y., Zhang, H., 2020. Evaluation of phosphate adsorption on zirconium/magnesium-modified bentonite. *J. Environ. Technol.* 41 (5), 586–602. <https://doi.org/10.1080/09593330.2018.1505966>.
- Lowry, O.H., Lopez, J.A., 1946. The determination of inorganic phosphate in the presence of labile phosphate esters. *J. Biol. Chem.* 162, 421–428.
- Mdlalose, L., Balogun, M., Setshedi, K., Chimuka, L., Chetty, A., 2018. Adsorption of phosphates using transition metals-modified bentonite clay. *Sep. Sci. Technol.* 54 (15), 2397–2408. <https://doi.org/10.1080/01496395.2018.1547315>.
- Milonjić, S.K., Kopečni, M.M., Ilić, Z.E., 1983. The point of zero charge and adsorption properties of natural magnetite. *J. Radioanal. Chem.* 78, 15–24. <https://doi.org/10.1007/BF02519745>.
- Młodzińska, E., Zboińska, M., 2016. Phosphate uptake and allocation - a closer look at *Arabidopsis thaliana* L. and *Oryza sativa* L. *Front. Plant Sci.* 7. <https://doi.org/10.3389/fpls.2016.01198>. 1198–1198.
- Mollah, M.Y.A., Morkovsky, P., Gomes, J.A.G., Kesmez, M., Parga, J., Cocke, D.L., 2004. Fundamentals, present and future perspectives of electrocoagulation. *J. Hazard. Mater.* 114 (1–3), 199–210. <https://doi.org/10.1016/j.jhazmat.2004.08.009>.
- Motulsky, H.J., Ransnas, L.A., 1987. Fitting curves to data using nonlinear regression: a practical and nonmathematical review. *FASEB J.* 1, 365–374.
- Nakamura, Y., Awai, K., Masuda, T., Yoshioka, Y., Takamiya, K.-i., Ohta, H., 2005. A novel phosphatidylcholine-hydrolyzing phospholipase C induced by phosphate starvation in *Arabidopsis*. *J. Biol. Chem.* 280, 7469–7476. <https://doi.org/10.1074/jbc.M408799200>.
- Parr, J.F., Norman, A.G., 1964. Effects of nonionic surfactants on root growth and cation Uptake1. *Plant Physiol.* 39 (3), 502–507. <https://doi.org/10.1104/pp.39.3.502>.
- Peng, Y., Sun, Y., Sun, R., Zhou, Y., Tsang, D.C.W., Chen, Q., 2019. Optimizing the synthesis of Fe/Al (Hydr)oxides-Biochars to maximize phosphate removal via response surface model. *J. Clean. Prod.* 237, 117770. <https://doi.org/10.1016/j.jclepro.2019.117770>.
- Péret, B., Clément, M., Nussaume, L., Desnos, T., 2011. Root developmental adaptation to phosphate starvation: better safe than sorry. *Trends Plant Sci.* 16 (8), 442–450. <https://doi.org/10.1016/j.tplants.2011.05.006>.
- Putro, J.N., Ismadji, S., Gunarto, C., Soetaredjo, F.E., Ju, Y.H., 2019. Effect of natural and synthetic surfactants on polysaccharide nanoparticles: hydrophobic drug loading, release, and cytotoxic studies. *Colloids Surf. A Physicochem. Eng. Asp.* 578, 123618. <https://doi.org/10.1016/j.colsurfa.2019.123618>.
- Raghothama, K.G., 1999. Phosphate acquisition. *Annu. Rev. Plant Physiol. Plant Mol. Biol.* 50 (1), 665–693. <https://doi.org/10.1146/annurev.arplant.50.1.665>.
- Robalds, A., Dreijalte, L., Bikovens, O., Klavins, M., 2016. A novel peat-based biosorbent for the removal of phosphate from synthetic and real wastewater and possible utilization of spent sorbent in land application. *Desalin. Water Treat.* 57, 13285–13294. <https://doi.org/10.1080/19443994.2015.1061450>.
- Santoso, S.P., Laysandra, L., Putro, J.N., Lie, J., Soetaredjo, F.E., Ismadji, S., et al., 2017. Preparation of nanocrystalline cellulose-montmorillonite composite via thermal radiation for liquid-phase adsorption. *J. Mol. Liq.* 233, 29–37. <https://doi.org/10.1016/j.molliq.2017.02.091>.
- Sotomayor, F.J., Cychosz, K.A., Thommes, M., 2018. Characterization of Micro/Mesoporous materials by physisorption: concepts and case studies. *Acc. Mater. Surf. Res.* 3 (2), 34–50.
- Tanyol, M., Yonten, V., Demir, V., 2015. Removal of phosphate from aqueous solutions by chemical- and thermal-modified bentonite clay. *Water Air Soil Pollut.* 226, 269. <https://doi.org/10.1007/s11270-015-2538-8>.
- Xie, F., Dai, Z., Zhu, Y., Li, G., Li, H., He, Z., et al., 2016. Adsorption of phosphate by sediments in a eutrophic lake: Isotherms, kinetics, thermodynamics and the influence of dissolved organic matter. *Colloids Surf. A Physicochem. Eng. Asp.* 562, 16–25. <https://doi.org/10.1016/j.colsurfa.2018.11.009>.
- Xie, Q., Li, Y., Lv, Z., Zhou, H., Yang, X., Chen, J., Guo, H., 2017. Effective adsorption and removal of phosphate from aqueous solutions and eutrophic water by Fe-based MOFs of MIL-101. *Sci. Rep.* 7, 3316. <https://doi.org/10.1038/s41598-017-03526-x>.
- Yaghoobi-Rahni, S., Rezaei, B., Mirghaffari, N., 2017. Bentonite surface modification and characterization for high selective phosphate adsorption from aqueous media and its application for wastewater treatments. *J. Water Reuse Desal.* 7 (2), 175–186. <https://doi.org/10.2166/wrd.2016.212>.
- Yang, Q., Wang, X., Luo, W., Sun, J., Xu, Q., Chen, F., et al., 2018. Effectiveness and mechanisms of phosphate adsorption on iron-modified biochars derived from waste activated sludge. *Bioresour. Technol.* 247, 537–544. <https://doi.org/10.1016/j.biortech.2017.09.136>.
- Yang, F., Zhang, S., Sun, Y., Tsang, D.S.W., Cheng, K., Ok, Y.S., 2019. Assembling biochar with various layered double hydroxides for enhancement of phosphorus recovery. *J. Hazard. Mater.* 365, 665–673. <https://doi.org/10.1016/j.jhazmat.2018.11.047>.
- Yao, Y., Gao, B., Chen, J., Yang, L., 2013. Engineered biochar reclaiming phosphate from aqueous solutions: mechanisms and potential application as a slow-release fertilizer. *Environ. Sci. Technol.* 47 (15), 8700–8708. <https://doi.org/10.1021/es4012977>.
- Zhang, S., Du, Q., Cheng, K., Antonietti, M., Yang, F., 2020. Efficient phosphorus recycling and heavy metal removal from wastewater sludge by a novel hydrothermal humification-technique. *Chem. Eng. J.* 394, 124832. <https://doi.org/10.1016/j.cej.2020.124832>.